

Taking off the edge - simultaneous filament and end core formation

S. Heigl,^{1,2*} E. Hoemann,^{1,3} A. Burkert,^{1,2,3}

¹Universitäts-Sternwarte, Ludwig-Maximilians-Universität München, Scheinerstr. 1, 81679 Munich, Germany

²Excellence Cluster ORIGINS, Boltzmannstrasse 2, 85748 Garching, Germany

³Max-Planck Institute for Extraterrestrial Physics, Giessenbachstr. 1, 85748 Garching, Germany

Accepted XXX. Received YYY; in original form ZZZ

ABSTRACT

Simulations of idealised star-forming filaments of finite length typically show core growth which is dominated by two cores forming at its respective end. The end cores form due to a strong increasing acceleration at the filament ends which leads to a sweep-up of material during the filament collapse along its axis. As this growth mode is typically faster than any other core formation mode in a filament, the end cores usually dominate in mass and density compared to other cores forming inside a filament. However, observations of star-forming filaments often do not show this prevalence of cores at the filament edges. We use numerical simulations of accreting filaments forming in a finite converging flow to explore a possible mechanism which leads to a suppression of the end cores. While such a setup still leads to end cores that soon begin to move inwards, the continued accumulation of material outside of these makes a key difference: their positions now lie within the larger filamentary structure and not at its edges. This softens their inward gravitational acceleration as they are embedded by new material further out. As a result, these two cores do not grow as fast as expected for the edge effect and thus do not dominate over other core formation modes in the filament.

Key words: stars:formation – ISM:kinematics and dynamics – ISM:structure

1 INTRODUCTION

A vital step in the star-formation process is the fragmentation of gas from molecular clouds on scales of a few tens of parsecs down to individual star-forming cores with sizes of a few tenths of a parsec. Schneider & Elmegreen (1979) and Larson (1985) established the idea that this collapse does not happen directly but goes through an intermediate phase of filamentary fragmentation. Indeed, the dust observations of the Herschel space telescope (André et al. 2010) showed that molecular clouds are dominated by intricate networks of filaments which also are the locations where most cores are found (Arzoumanian et al. 2011; Könyves et al. 2015).

Many processes related to filament formation and their subsequent fragmentation are still unclear. Filamentary structure has been seen as a natural outcome of turbulent box simulations, with or without gravity (Vazquez-Semadeni 1994; Klessen & Burkert 2000; Padoan et al. 2001; Moeckel & Burkert 2015; Federrath 2016). These simulations have shown that they form by the compression of gas in the crossing of two planar shocks or as a consequence of dissipation at the end of the turbulent cascade (Kritsuk et al. 2013; Smith et al. 2014, 2016). The formation sites of stars are then given by the collapse of the largest overdensities which form along the filaments.

Nevertheless, simulations of individual, isolated filaments show a different morphology (Bastien 1983; Bastien et al. 1991; Clarke & Whitworth 2015; Seifried & Walch 2015) with strong overdensities forming at both ends of the filament. This is due to the gravita-

tional acceleration being the largest at the filament ends (Burkert & Hartmann 2004; Pon et al. 2011, 2012; Toalá et al. 2012; Clarke & Whitworth 2015), a concept which can be more generalised to more complex structures and which is known as so-called "gravitational focusing" (Burkert & Hartmann 2004; Hartmann & Burkert 2007; Li et al. 2016), where the magnitude of the gravitational acceleration scales with the curvature of the surface.

While there are observed cases of end dominated filaments (Zernickel et al. 2013; Kainulainen et al. 2016; Johnstone et al. 2017; Ohashi et al. 2018; Dewangan et al. 2019; Bhadari et al. 2020; Yuan et al. 2020; Cheng et al. 2021), the majority of observed filaments do not show a particular disposition to forming their most massive cores at their ends which can be due to several reasons. For instance, filaments forming in networks are interconnected and therefore do not have the density gradients at their ends required to form edge cores. Nevertheless, one would expect the ends of the network to enhance core formation. Moreover, it has been shown that if filaments form with low aspect ratios, large initial central overdensities or via filament mergers, the collapse of the gas is concentrated onto its centre (Keto & Burkert 2014; Seifried & Walch 2015; Hoemann et al. 2021), a morphology which has also been observed in large line-mass filaments (Kirk et al. 2013; Henshaw et al. 2014). Large central overdensities are however not expected in low-mass star forming filaments.

In this paper we present an additional process which suppresses dominant cores at the filament ends: the simultaneous migration of the forming end cores while the filament is under formation itself. In the turbulent formation regime, filaments form by colliding shocks leading to mass inflow on the cross-section of the shocks over a

* E-mail: heigl@usm.lmu.de

timescale which is given by the size of the inflow region and the shock velocity. In order to stabilise the filamentary structure we instead assume a radial inflow in our idealised simulations. Such radial accretion flows have been observed in many filaments (Schneider et al. 2010; Kirk et al. 2013; Palmeirim et al. 2013; Shimajiri et al. 2019; Bonne et al. 2020) and typically show estimated accretion rates of around $10 - 100 M_{\odot} \text{ pc}^{-1} \text{ Myr}^{-1}$ and accretion velocities of the order of $0.25 - 1.0 \text{ km s}^{-1}$. If we assume a shock inflow region feeding the filament of around 0.5 pc , this would lead to a sustained inflow of material on timescales of $0.5\text{--}2 \text{ Myr}$. We demonstrate below that, while a filament is forming in such a sustained accretion flow, end cores will indeed begin to form and start migrating inwards while new material reforms the filament behind them. As we will show, this results in a suppression of the runaway growth of these cores and to core formation within the whole filament on roughly the same timescale.

The sections of the paper are organised as follows: section 2 discusses the basic physical principles which lead to the formation of cores at the filament ends. The numerical principles and initial conditions of the simulations are introduced in section 3 and their results are presented and discussed in section 4. We draw the conclusions and summarise the results in section 5.

2 BASIC CONCEPTS

While the edge-effect is not the only mode of core formation in filaments, it usually is the fastest. The end cores form at the position of the strong density gradient located at the ends of a filament due to the sharp increase in gravitational acceleration. Assuming a filament has a constant density ρ , a total length of L , a radius R and that the filament is directed along the x -axis, this acceleration is given by (Burkert & Hartmann 2004):

$$a_x = -2\pi G \rho \left[2x - \sqrt{R^2 + (L/2 + x)^2} + \sqrt{R^2 + (L/2 - x)^2} \right] \quad (1)$$

with G being the gravitational constant. The acceleration on the ends increases steeply for large aspect ratios which can be seen, for instance, in (Pon et al. 2012). For $x = L/2$ and large lengths ($L \gg R$) this acceleration equals:

$$a_x = -2\pi G \rho R. \quad (2)$$

In fact the acceleration increase is even stronger for more centralised radial profiles (Hoemann et al. in prep) such as the isothermal hydrostatic cylindrical profile (Stodólkiewicz 1963; Ostriker 1964):

$$\rho(r) = \frac{\rho_c}{\left(1 + (r/H)^2\right)^2} \quad (3)$$

where r is the cylindrical radius and ρ_c is its central density. The radial scale height H is given by the term:

$$H^2 = \frac{2c_s^2}{\pi G \rho_c} \quad (4)$$

where c_s is the isothermal sound speed. This profile can only support a maximum mass per length in hydrostatic equilibrium. The maximum value is calculated by integrating the profile radially to infinity:

$$\left(\frac{M}{L}\right)_{\text{crit}} = \frac{2c_s^2}{G} \quad (5)$$

and one can define the parameter f_{cyl} which gives the value of the current line-mass compared to the critical value (Fischera & Martin

2012):

$$f_{\text{cyl}} = \left(\frac{M}{L}\right) / \left(\frac{M}{L}\right)_{\text{crit}}. \quad (6)$$

3 NUMERICAL SET-UP

We ran our simulation with the code `RAMSES` (Teyssier 2002) using a second-order Godunov scheme to solve the conservative form of the discretised Euler equations on an Cartesian grid. We applied the MUSCL scheme (Monotonic Upstream-Centred Scheme for Conservation Laws van Leer 1979) in combination with the HLLC-Solver (Harten-Lax-van Leer-Contact Toro et al. 1994) and the multidimensional MC slope limiter (monotonized central-difference van Leer 1977).

The formation and gravitational evolution of a finite-sized filament is simulated taking into account mass accretion from the surrounding. This is a key difference to previous simulations (Bastien 1983; Bastien et al. 1991; Clarke & Whitworth 2015; Seifried & Walch 2015) that assumed an already existing mature filament and that followed its subsequent collapse. We do this by setting up a cylindrical inflow zone with a radius that is set in the y - z dimension and define a constant radial accretion flow onto the central x -axis, similar to the initial conditions of Heigl et al. (2018) and Heigl et al. (2020). In contrast to the former cases however, all boundaries of the box are set to open and we do not use a periodic boundary condition in x direction. In addition we limit the accretion flow to the central section of the box with a size of 0.6 times the box length. We choose the box to have a physical size of 2.0 pc resulting in an accretion zone with a radius of 1.0 pc and a length of 1.2 pc . The gas is set to be isothermal with a temperature of 10 K . Its initial density in the box and that of the accretion flow is set to $3.92 \times 10^{-22} \text{ g cm}^{-3}$, corresponding to a number density of about 100 cm^{-3} for a molecular weight of $\mu = 2.36$. In order to break the symmetry, we introduce density perturbations in the initial density and in the inflow on the order of 10% which allows the driving of turbulent motions. As shown in Heigl et al. (2018), the amplitude of the turbulence does not depend on the strength of the initial perturbation. The inflow velocity is set to a value of 7.51 km s^{-1} , which corresponds to a Mach number of 4.0 for 10 K gas. The resulting accretion rate is therefore about $27.9 M_{\odot} \text{ pc}^{-1} \text{ Myr}^{-1}$ which is consistent with predicted and observed accretion rates and velocities.

As the filament diameter itself is only a fraction of the total box size and as we are not interested in the details of the accretion flow itself, we employ adaptive mesh refinement (AMR) in order to speed up the simulation by increasing the resolution inside the filament and keeping the resolution low in the ambient medium. We vary the resolution level from 8 to 12 which means that our base grid has a resolution of 256^3 , corresponding to a cell size of $7.8 \times 10^{-3} \text{ pc}$, whereas our filament is resolved by a resolution of 4096^3 , corresponding to a cell size of $4.9 \times 10^{-4} \text{ pc}$. As a refinement condition we use the Truelove criterion (Truelove et al. 1997) increasing the resolution as soon as the Jeans length is not resolved by 256 cells. We choose an aggressive refinement value of 256 in order to guarantee that the filament is resolved fully with our highest resolution. We stop the simulation as soon as a core collapses and we do not fulfill the Truelove criterion for our highest refinement level anymore.

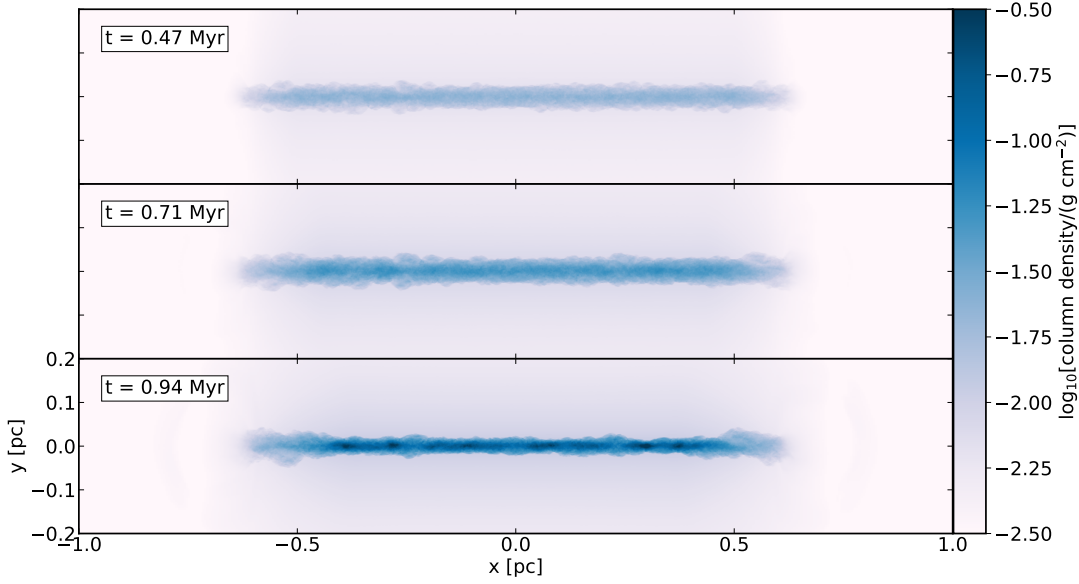


Figure 1. Overview of the simulation given by the density projection along the z -axis at different points in time. The radial accretion flow forms a turbulent filament which forms regularly spaced cores along its axis. The y -axis label is the same for every panel.

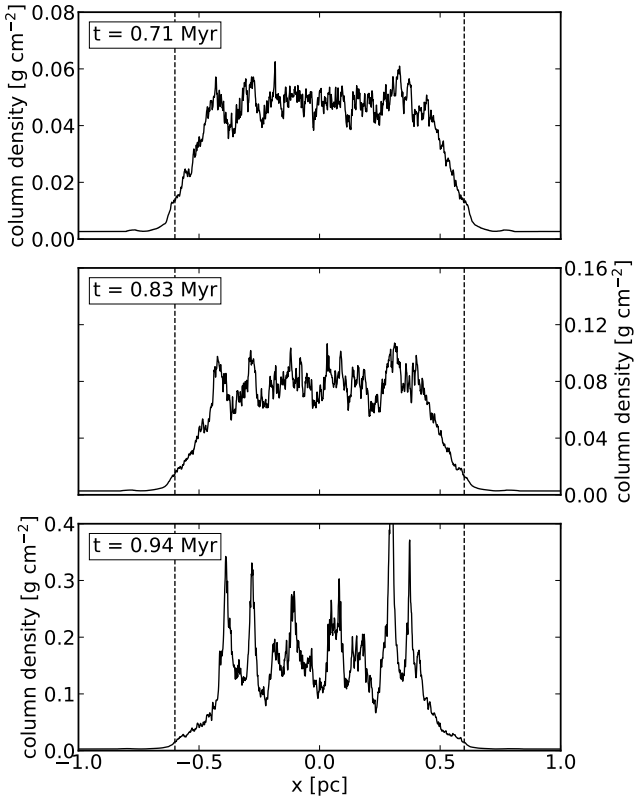


Figure 2. Time evolution of the column density in z direction along the central x -axis. The inflow region is marked by the vertical dashed lines. In contrast to developing dominant edge cores, the inner dense region stays relatively even. The filament contracts over time and forms equally dense cores along its axis. The x -axis label applies to every panel.

4 SIMULATION RESULT

Here we provide a detailed analysis of the simulation results starting with an overview of the evolution of the filament in [Figure 1](#). We plot the column density along the z -axis assuming our gas is optically thin. The different panels show different time steps of the simulation. As the material streams to the box centre it forms a filament which linearly gains mass over time. In addition, the inflow stabilises the filament against radial expansion. One can clearly see the turbulent nature of the gas which is driven by the dissipative accretion shock and a smooth density gradient at the two end points of the filament ends extending into the ambient medium. A tentative imprint of the inflow region can be seen in column density as slightly darker region around the filament itself. Other than its straight form due to the nature of how we defined the filament accretion, the visual impression closely resembles observed filamentary structure.

While a pre-defined, non-accreting filament would immediately start forming end cores, most of the evolution of the accreting filament is uneventful. As it grows in mass over time it becomes denser while retaining a relatively soft gradient in column density to the ambient medium. After about 0.7 Myr, cores condense out of the filament material with none being particularly dominant compared to the others. The last snapshot of the simulation is shown in the third panel where one can see several cores along the filament with similar spacing. Note that the outermost cores do not coincide with the filament ends.

In addition to the slices, we also show column density cuts along the central axis in [Figure 2](#) where the core evolution can be seen in more detail. The first panel shows the earliest stage of overdensities forming in the filament. Although material is accreted in the region between $x = -0.6$ and $x = 0.6$, one can already see that the densest part is shorter and forms a central dense region which contracts over time. While for a non-accreting filament this contraction would concentrate material in the filament ends, in this case the accreting

filament shows a homogeneous increase along its axis with only small density fluctuations. The next panel shows a time step where several cores have formed. While there are also two cores forming at the end of the inner density enhancement, these do not form earlier than the rest and have similar column densities as the other cores. While the inner dense region contracts along the filament axis, one can see that the continuous inflow brings in new material around its ends. This leads to a softening of the gravitational attraction at the position of the end cores as can be seen in Figure 3. Here we show the measured gravitational acceleration for the same time step along the filament in the simulation as the solid curve together with the analytical prediction of Equation 1 where we use the length, the mean density and the mean radius of the dense inner region. As one can see, the prediction agrees very well with the measured acceleration. Only at the end of the dense inner region, where the end cores form, it differs strongly. As the ends of the inner region are more and more embedded in newly accreted material, the potential at their position matches more a region contained inside a filament. As the new density gradient is very shallow, the new ends are evenly accelerated instead of leading to a sweep-up of material. The last panel of Figure 2 shows the last time step of the simulation where one of the cores begins to collapse leading to a drastic increase in its central column density. Interestingly, it is not one of the outermost ones as one would expect for an edge dominated filament but the second from the right. Again, neglecting the collapsing one, all cores have similar central column densities albeit with a possible tendency of the outer cores to be slightly denser.

An interesting consequence of the radial compression of the gas is that a small amount of material is pushed out at the filament ends due to the pressure gradient from the dense compressed material to the ambient medium. This leads to a small shocked region surrounding both filament ends. Although this feature is very hard to detect in the column density of Figure 1, it can be seen in the density slice through the centre of the filament shown in Figure 4. In addition to the density, we also show the direction of the velocity vectors in the plane of the slice overlaid as streamlines. One can see the inflow region accreting onto the filament, the ambient medium being gravitationally pulled towards the filament and the two outflow regions pushing against it. While the density of the outflow regions is very thin, shock fronts form where they hit and compress the ambient medium. Whether such outflow features can be detected in observations is an interesting question, its thin density however makes such observations challenging. Note that the outflows do not affect the overall evolution of the filament itself as the mass loss rate of about $\sim 0.1 M_{\odot} \text{ Myr}^{-1}$ at both ends is negligible small compared to the total mass accretion rate of $16.7 M_{\odot} \text{ Myr}^{-1}$.

A key question of filamentary fragmentation theory and of star formation is the existence of a quasi-regular core spacing. This mode of fragmentation has been predicted by hydrostatic models as there exists a dominant mode for which the growth time scale of the overdensities is the fastest. Observations of core spacing have been inconclusive with several studies showing lower separations than expected (André et al. 2010; Kainulainen et al. 2013; Teixeira et al. 2016) with some agreeing with the predictions (Beuther et al. 2015; Contreras et al. 2016; Kainulainen et al. 2016). Consequently, the core separation in our simulations is of considerable interest.

There are two major complications to verify the theoretical predictions not only in simulations but also in observations. On the one hand, the dominant fragmentation length depends on the instantaneous average line-mass of the filament. If it varies over time, as is the case for an accreting filament, one can only measure the current average line-mass at a single point in time and not the line-mass the

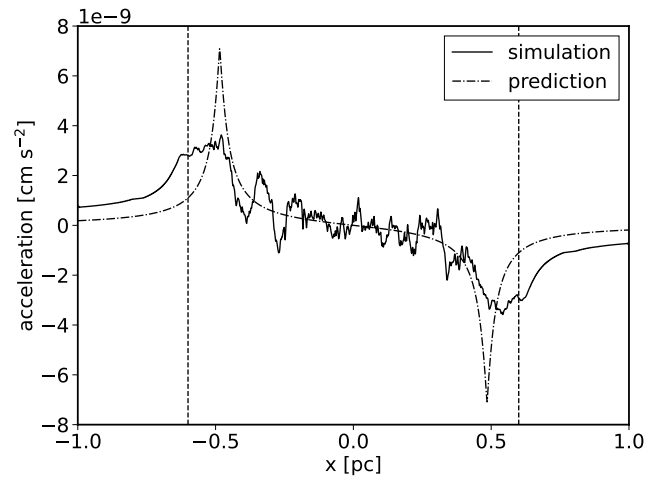


Figure 3. Gravitational acceleration along the filament axis for $t=0.83 \text{ Myr}$. The solid curve shows the measured acceleration in the simulation while the dashed-dotted curve is the analytic prediction of Equation 1 for the dense inner region. The inflow region is marked by the dashed vertical lines. There is a considerable softening of the acceleration at the positions of the end cores.

filament had when the cores began forming. On the other hand, the length of the filament and the distance between cores will decrease over time due to the gravitational collapse along its axis. At a single point in time, one can only measure the current distance, further complicating the comparison.

To this end, we analyse the average core separation for varying accretion rates in our simulations over time and compare them with the hydrostatic prediction. In order to address the effects mentioned above, we use the method of counting the number of cores and measuring the changing length of the inner dense region to derive their mean separation and compare it to the theoretical dominant fragmentation time taking into account its current line-mass. As one can see from Figure 2 one can count the number of cores by determining the number of overdensities. However, there is no good general criteria for classifying a particular overdensity as a core as they are in varying states of formation. In order to improve our counting method we take into account not only the column density but also the physical density and the line-mass along the filament and only use overdensities which give a clear signal in all three quantities. We determine the length of the inner dense region along which the fragmentation is happening by the outer end of the forming end cores which show a clear rise in column density as can be seen in Figure 2. Since the inner dense region is not defined at the start of the simulation, we use the value of the total inflow region. As we do not see any core mergers happening, the average separation is then given by the current length of the inner dense region, divided by the number of cores minus one in order to take into account the two edge cores.

Furthermore, in order to obtain a better statistical sample we repeat every simulation for a given accretion rate ten times and take the mean and the standard deviation of the number of cores. The mean core number for increasing accretion rates of 10.5, 21.0 and $41.9 M_{\odot} \text{ pc}^{-1} \text{ Myr}^{-1}$ is 2.5, 5.1 and 10.2 and their standard deviation is 0.5, 0.8 and 1.4, respectively. We measure the average line-mass and length of the inner dense region at several points in time and verify that they do not vary much from simulation to simulation and plot the resulting mean separation together with the prediction

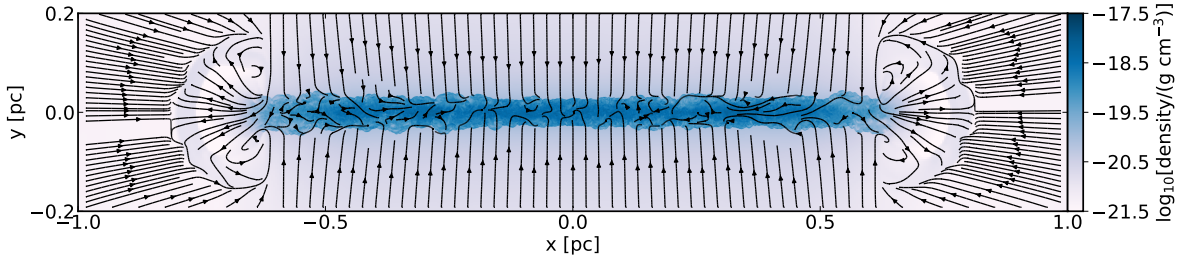


Figure 4. Density slice through the centre of the filament at 0.71 Myr. The streamlines show the direction of the velocity in the plane of the slice. One can see that material at the filament ends is flowing into the ambient medium where it forms shock fronts.

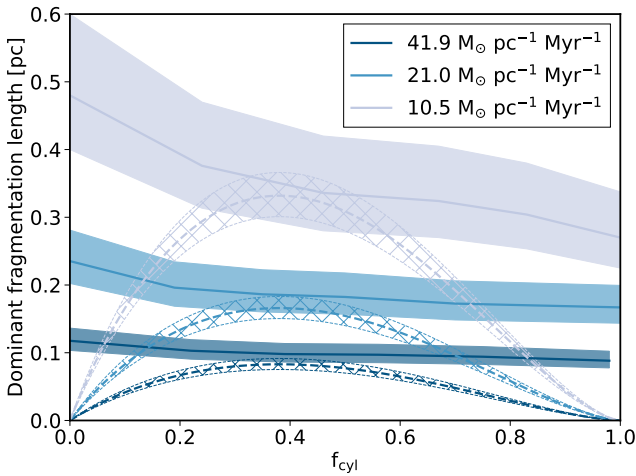


Figure 5. Dominant core separation for different accretion rates as function of the line-mass. The solid lines show the calculated mean separations in the simulation by counting the number of cores and measuring the length of the dense inner region. The error bars show the standard deviation of the number of cores in ten different simulations varying the initial random seed. The theoretical prediction of the dominant mode is given by the dashed lines for different accretion rates together with the error resulting from the observed variation of the turbulent Mach number.

in Figure 5. The prediction is shown as function of the line-mass calculated from table E.1 of Fischera & Martin (2012) as dashed lines and take into account the radius corrections for accretion driven turbulence given by the balance of external ram pressure and internal turbulent pressure as described in Heigl et al. (2020):

$$R = \frac{2c_s^2 (1 + \mathcal{M}_t^2)}{\pi \rho_0 R_0 G (1 + \mathcal{M}_a^2)} (f_{\text{cyl}} (1 - f_{\text{cyl}})). \quad (7)$$

where the accretion of constant mass per time is given by a density profile

$$\rho(R) = \frac{\rho_0 R_0}{R} \quad (8)$$

defined by the inflow of material of density ρ_0 normalised at a radius R_0 with \mathcal{M}_a and \mathcal{M}_t being the respective accretion and turbulent Mach numbers. We use an accretion Mach number of 6.0 as for a box size of 2.0 pc the gravitational acceleration on the gas starting at the edge of the box can already increase the infall velocity significantly

for lower accretion Mach numbers. This could potentially influence the resulting turbulent Mach number as it results directly from the accreted kinetic energy. For our choice of Mach 6.0 however, we do not see a significant acceleration and the accretion rate is then varied by adjusting the density ρ_0 . We include an errorbar in the predictions shown as the crossed-out area as we do see some variation in the turbulent Mach number in the simulations of Heigl et al. (2020) on the order of 10% for the same accretion Mach number. Note, that if we do not include the turbulent correction term for the radius, the predicted fragmentation length deviates strongly and is about half of the shown values.

As one can see the measured fragmentation lengths match well with the peak of the predicted separations for values of around $f_{\text{cyl}} \approx 0.3 - 0.5$. This could indicate that the cores are seeded at a point in time where the filament has approximately line-mass. However, this is only a first order approach as the mode on which cores would grow the fastest is constantly changing. Nevertheless, one can see from the form of the curves shown in Figure 5 that close to the peak the values of the dominant fragmentation length remain very similar. As an accreting filament is growing approximately linearly in line-mass, it spends a considerable amount of its lifetime at this dominant fragmentation length. For smaller and larger line-masses the change in dominant fragmentation length is much stronger. Therefore, perturbations seeded in this line-mass region are able to grow on this fragmentation length longer than at any other point in the filament's evolution. This could lead to core growth which is strong enough in the beginning to exceed other modes at later times even if the dominant fragmentation length is constantly changing. In order to verify our theory we calculate the time spent by the filament at $f_{\text{cyl}} \approx 0.3 - 0.5$ and compare it to the mean e-folding time of the dominant fragmentation length at these values. Neglecting the effect of the collapse of the inner dense region on the line-mass, the time spent at these values is given by the time which it takes for f_{cyl} to grow from 0.3 to 0.5 which is given by the accretion rate. The e-folding timescales of the dominant fragmentation length are also given in table E.1 of Fischera & Martin (2012). For all our simulated cases, the timescales match exceptionally well. For accretion rates of 10.5, 21.0 and 41.9 $M_\odot \text{ pc}^{-1} \text{ Myr}^{-1}$ the time the filament takes to grow from $f_{\text{cyl}} = 0.3$ to 0.5 is given by 0.31, 0.16 and 0.08 Myr, while the mean dominant e-folding time is 0.32, 0.16 and 0.08 Myr, respectively. This means that cores seeded in this line-mass region have enough time to grow for about an e-folding time and exceed later modes as these have less time to grow at their respective dominant fragmentation length. Therefore, we see a tentative indication that

the analytic prediction of the hydrostatic model is consistent with the fragmentation in accreting filaments.

In general, increasing the accretion rate leads to the formation of more cores. This is to be expected as a larger accretion rate leads to a larger ram pressure onto the filament which increases its central density which in turn lowers the dominant fragmentation length. However, from the core separation alone one cannot derive the accretion rate as the same ram pressure can be achieved by varying numbers of accretion density and velocity. Nevertheless, one can use the observed core separation as an indicator of the ambient pressure. As one can see in Figure 5, at least for larger accretion rates, the line-mass of the filament grows faster than the central dense region contracts which results in a flattening of the measured core separation for larger values of the filament line-mass. If one now assumes that the cores are seeded at values of $f_{\text{cyl}} \approx 0.3 - 0.5$, one can in principle estimate the ambient pressure of the surrounding medium leading to a corresponding dominant fragmentation length.

5 DISCUSSION AND CONCLUSIONS

While our simulations show that a continuous accretion does prevent the formation of dominant end cores, several additional questions remain.

An intriguing puzzle is the tendency of observations to find narrower core separations in large line-mass filaments than what is predicted by theory (André et al. 2010; Kainulainen et al. 2013; Teixeira et al. 2016). Our analysis of expected fragmentation lengths presented in Figure 5 shows that for large line-masses the line-mass itself grows faster than the inner region contracts. Therefore, in contrast to observations, the predicted fragmentation length is usually shorter than what we measure in simulations. This could be an indication that such a hydrostatic model is not applicable for all filaments.

A surprising side effect of the model is the creation of outflows at the filament ends. This effect however could be reduced by non homogeneous inflows with low density at the shock front ends. Due to their low density and mass loading, these outflow would be very hard to detect and as far as we know there is no observation of such an phenomena to date. A possible tracer of the outflow would be the shock heating or chemical shock traces in the ambient medium as the material streams out with large velocities.

Finally, it will be interesting to explore whether our results remain valid in the case of planar accretion flows instead of radial geometries. Depending on the extent, a planar shock will not create a filamentary morphology but lead to a sheet between the shock fronts. However, as soon as enough material has been concentrated and gravity takes over, this sheet could collapse and be collected into a filamentary structure. We will explore if this mode of filament formation shows the same effect on end core formation as presented here in a future study.

To summarise, we have presented a numerical study on the simultaneous filament and end core formation. In this scenario the filament is formed by a converging radial flow which drives turbulent motions inside the filament. We have shown that while edge cores do form at the ends of the central dense region, they do not dominate over the cores formed by regular perturbation growth. This is due to the material which is replenished continuously from the inflow outside of the contracting inner region which leads to a reduced gravitational acceleration at its ends and a soft edge morphology. Comparing the observed core separation to the analytical prediction at different line-masses shows a tentative agreement that cores are seeded at $f_{\text{cyl}} \approx 0.3 - 0.5$. The comparison is not straight-forward

due to a continuously shifting dominant fragmentation length over time, however an accreting filament spends a considerable amount of time in this line-mass region where the dominant fragmentation length only changes slightly. This means that cores seeded at these values have about an e-folding timescale to grow and therefore exceed later core formation modes. Independent of the core separation, we presented a valid mechanism to form a filament morphology which is not dominated by the edge effect as was the goal of the paper.

ACKNOWLEDGEMENTS

We thank the whole CAST group for helpful comments and discussions. This research was supported by the Excellence Cluster ORIGINS which is funded by the Deutsche Forschungsgemeinschaft (DFG, German Research Foundation) under Germany's Excellence Strategy – EXC-2094 – 390783311.

DATA AVAILABILITY

The data underlying this article will be shared on reasonable request to the corresponding author.

REFERENCES

- André P., et al., 2010, *A&A*, **518**, L102
- Arzoumanian D., et al., 2011, *A&A*, **529**, L6
- Bastien P., 1983, *A&A*, **119**, 109
- Bastien P., Arcoragi J.-P., Benz W., Bonnell I., Martel H., 1991, *ApJ*, **378**, 255
- Beuther H., Ragan S. E., Johnston K., Henning T., Hacar A., Kainulainen J. T., 2015, *A&A*, **584**, A67
- Bhadari N. K., Dewangan L. K., Pirogov L. E., Ojha D. K., 2020, *ApJ*, **899**, 167
- Bonne L., et al., 2020, *A&A*, **641**, A17
- Burkert A., Hartmann L., 2004, *ApJ*, **616**, 288
- Cheng Y., et al., 2021, *ApJ*, **916**, 78
- Clarke S. D., Whitworth A. P., 2015, *MNRAS*, **449**, 1819
- Contreras Y., Garay G., Rathborne J. M., Sanhueza P., 2016, *MNRAS*, **456**, 2041
- Dewangan L. K., Pirogov L. E., Ryabukhina O. L., Ojha D. K., Zinchenko I., 2019, *ApJ*, **877**, 1
- Federrath C., 2016, *MNRAS*, **457**, 375
- Fischera J., Martin P. G., 2012, *A&A*, **542**, A77
- Hartmann L., Burkert A., 2007, *ApJ*, **654**, 988
- Heigl S., Burkert A., Gritschneider M., 2018, *MNRAS*, **474**, 4881
- Heigl S., Gritschneider M., Burkert A., 2020, *MNRAS*, **495**, 758
- Henshaw J. D., Caselli P., Fontani F., Jiménez-Serra I., Tan J. C., 2014, *MNRAS*, **440**, 2860
- Hoemann E., Heigl S., Burkert A., 2021, *MNRAS*, **507**, 3486
- Johnstone D., et al., 2017, *ApJ*, **836**, 132
- Kainulainen J., Ragan S. E., Henning T., Stutz A., 2013, *A&A*, **557**, A120
- Kainulainen J., Hacar A., Alves J., Beuther H., Bouy H., Tafalla M., 2016, *A&A*, **586**, A27
- Keto E., Burkert A., 2014, *MNRAS*, **441**, 1468
- Kirk H., Myers P. C., Bourke T. L., Gutermuth R. A., Hedden A., Wilson G. W., 2013, *ApJ*, **766**, 115
- Klessen R. S., Burkert A., 2000, *ApJS*, **128**, 287
- Könyves V., et al., 2015, *A&A*, **584**, A91
- Kritsuk A. G., Lee C. T., Norman M. L., 2013, *MNRAS*, **436**, 3247
- Larson R. B., 1985, *MNRAS*, **214**, 379
- Li G.-X., Burkert A., Megeath T., Wyrowski F., 2016, arXiv e-prints, p. arXiv:1603.05720
- Moeckel N., Burkert A., 2015, *ApJ*, **807**, 67

- Ohashi S., Sanhueza P., Sakai N., Kandori R., Choi M., Hirota T., Nguyen-Lu'o'ng Q., Tatematsu K., 2018, [ApJ](#), **856**, 147
- Ostriker J., 1964, [ApJ](#), **140**, 1056
- Padoan P., Juvela M., Goodman A. A., Nordlund Å., 2001, [ApJ](#), **553**, 227
- Palmeirim P., et al., 2013, [A&A](#), **550**, A38
- Pon A., Johnstone D., Heitsch F., 2011, [ApJ](#), **740**, 88
- Pon A., Toalá J. A., Johnstone D., Vázquez-Semadeni E., Heitsch F., Gómez G. C., 2012, [ApJ](#), **756**, 145
- Schneider S., Elmegreen B. G., 1979, [ApJS](#), **41**, 87
- Schneider N., Csengeri T., Bontemps S., Motte F., Simon R., Hennebelle P., Federrath C., Klessen R., 2010, [A&A](#), **520**, A49
- Seifried D., Walch S., 2015, [MNRAS](#), **452**, 2410
- Shimajiri Y., André P., Palmeirim P., Arzoumanian D., Bracco A., Könyves V., Ntormousi E., Ladjelate B., 2019, [A&A](#), **623**, A16
- Smith R. J., Glover S. C. O., Klessen R. S., 2014, [MNRAS](#), **445**, 2900
- Smith R. J., Glover S. C. O., Klessen R. S., Fuller G. A., 2016, [MNRAS](#), **455**, 3640
- Stodólkiewicz J. S., 1963, *Acta Astron.*, **13**, 30
- Teixeira P. S., Takahashi S., Zapata L. A., Ho P. T. P., 2016, [A&A](#), **587**, A47
- Teyssier R., 2002, [A&A](#), **385**, 337
- Toalá J. A., Vázquez-Semadeni E., Gómez G. C., 2012, [ApJ](#), **744**, 190
- Toro E., Spruce M., Speares W., 1994, [Shock Waves](#), **4**, 25
- Truelove J. K., Klein R. I., McKee C. F., Holliman II J. H., Howell L. H., Greenough J. A., 1997, [ApJ](#), **489**, L179
- Vazquez-Semadeni E., 1994, [ApJ](#), **423**, 681
- Yuan L., et al., 2020, [A&A](#), **637**, A67
- Zernickel A., Schilke P., Smith R. J., 2013, [A&A](#), **554**, L2
- van Leer B., 1977, [Journal of Computational Physics](#), **23**, 276
- van Leer B., 1979, [Journal of Computational Physics](#), **32**, 101

This paper has been typeset from a \LaTeX file prepared by the author.